Conducted Noise Prediction for DC–DC Converter by Noise Source Model Accounting for Switching Fluctuation

Shuqi Zhang, *Student Member, IEEE*, Kengo Iokibe, *Member, IEEE*, and Yoshitaka Toyota, *Member, IEEE*

***Abstract*—The switching fluctuation of a dc–dc converter causes jitter and makes the conducted noise time-variant. Averaging-mode measurement with an oscilloscope or other instruments partially removes higher-frequency noise. Therefore, switching fluctuation affects the accuracy of noise prediction in using a black-box noise source model with measurement-based parameter identification. To address this issue, we proposed an approach to address the switching fluctuation effect on conducted emissions from the dc–dc converter. First, we investigate the effect of switching fluctuation by studying the difference between noise signals with and without fluctuation and estimating the reduction due to fluctuation. Then, to facilitate model parameter identification, we focus on the peak detected noise signal and improve the prediction accuracy of the peak detected noise by decomposing the measured noise signal into ripple noise and turn-ON and turn-OFF spike noises. As a result, the peak detected noise spectrum after removing switching fluctuation can be predicted within a 3-dB error up to 200 MHz. Our experimental results show that the noise spectrum predicted by accounting for the reduction due to switching fluctuation agrees well with the spectrum obtained by averaging-mode measurement.**

***Index Terms*—Black-box method, conducted emission, equivalent noise source model, jitter, switching fluctuation.**

I. Introduction

MODELING of the electromagnetic interference (EMI) due to switching of a power supply has become a challenging but important topic in recent years. Two main methods are used to predict the EMI from electronic devices. The first is the partial element equivalent circuit method [1], in which the parasitic element of the entire propagation path can be obtained by commercial software. However, the cost of this method increases greatly for complex components and systems. The second method treats the noise source and propagation path as a black-box model that uses a Norton or Thevenin equivalent circuit with noise impedance and noise sources to represent the EMI characteristics. The prediction process is relatively simple when the details of the electronics are unknown.

Manuscript received 9 March 2022; revised 20 July 2022, 18 October 2022, and 21 December 2022; accepted 6 January 2023. Date of publication 19 January 2023; date of current version 13 June 2023. *(Corresponding author: Yoshitaka Toyota)*

The authors are with the Graduate School of Natural Science and Technology, Okayama University, Okayama 700-8530, Japan (e-mail: pypl4x2y@s.okayama-u.ac.jp; iokibe@okayama-u.ac.jp; toyota@okayama-u.ac.jp).

Color versions of one or more figures in this article are available at https://doi.org/10.1109/TEMC.2023.3236674.

Digital Object Identifier 10.1109/TEMC.2023.3236674

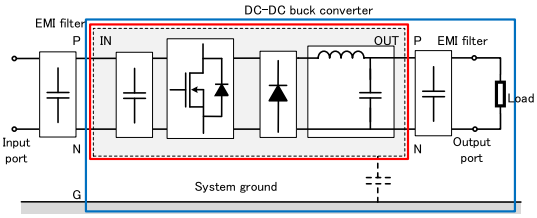

Fig. 1. DC–DC converter with a load placed above the system ground.

There have been many studies on EMI prediction based on the black-box method [2], [3], [4], [5], [6], [7], [8], [9], [10], [11], [12], [13], [14], [15], [16], [17], [18], [19], [20], [21], [22]. Liu et al. proposed an EMI model called the modular-terminal-behavioral (MTB) model [3]. In another approach, the insulated-gate bipolar transistor phase leg conducted emission was modeled by a Norton equivalent noise emission model. Baisden [4] and Bishnoi et al. [5], [6] developed the general terminal modeling (GTM) method as an extension of the MTB model for wider applications, such as converter and dc-motor drive noise prediction. Both the prediction accuracy and frequency range were improved in the GTM model by applying the insertion loss method proposed by Zhang et al. [7]. A shunt impedance was used to determine the boost converter noise parameters of the noise source, and the noise impedance identification procedure was simplified. Furthermore, that kind of model was extended to system-level modeling in [9], [10], and [11]. The black-box EMI model is seen as a good tool for predicting system-level EMI. And the noise parameter identification approach was studied in [12]. Zhang et al. [13] developed a model of a four-port network for mixed-mode noise by considering the physical meaning of a converter. Fig. 1 illustrates a dc–dc converter with a load placed above the system ground. The GTM model is constructed by focusing on the blue box in Fig. 1, which yields the model shown in Fig. 2(a). The GTM model can predict not only the normal-mode (NM) noise but also the common-mode (CM) noise for a fixed load but it cannot address the load dependence.

Accordingly, to address the load dependence, the red box in Fig. 1 can be modeled by removing the load. The black-box noise source model was first proposed to focus only on the NM noise [14]. It was then modified as shown in Fig. 2(b) [15] to improve the prediction accuracy by more than 20 dB. As a result, the conducted noise at both the input port and the output port can be predicted up to 200 MHz. Subsequently, the load effect was

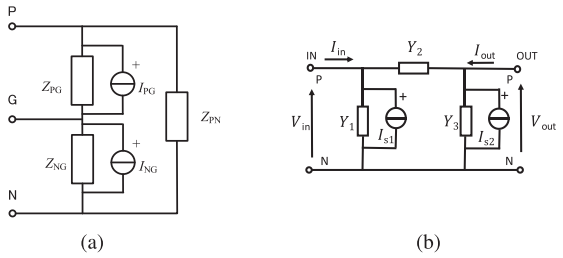

Fig. 2. Two-port noise source models including and excluding the load. (a) Load included. (b) Load excluded.

investigated [16]. As long as a semiconductor device mounted on a printed circuit board (PCB) is well-grounded, we can focus only on the differential-mode (DM) noise.

However, one problem with the behavior modeling method is that the EMI from a dc–dc converter is not time-invariant because of its switching fluctuation. The time-variant behavior of the dc–dc converter should thus be examined, and several studies have addressed this problem [17], [18], [19], [20], [21], [22], [23]. The above technique thus requires keeping the converter in an approximately time-invariant working condition by some approach, such as keeping the input voltage and load at fixed values and using an averaging mode to measure the noise signal. Rebholz et al. [17] showed that small jitter could be eliminated through time-domain averaging of 10–200 signals but the result was limited to periodic noise sources. Sanchez et al. [18] proposed a model to predict nonstationary and impulsive interferences from a switching power supply. Trinchero et al. [19], [20] developed an enhanced Norton model to predict DM noise by incorporating the periodic time-varying activity of the switching. The frequency range and accuracy were limited with the Fourier expansions of the admittance matrix. Shen et al. considered the stochastic behavior of a dc–dc converter and proposed the use of a custom PCB to characterize its noise signal characteristics. They predicted both the averaged spectrum result and the maximized spectrum from the converter [21]. They found that the maximized spectrum exceeded the averaged spectrum by 10 dB at frequencies above 10 MHz because the intentional random modulation or oscillator instability reduced the peak level of the EMI spectrum.

The above studies tried to eliminate the random noise due to switching fluctuation by averaging measurements. However, the use of an averaging mode reduces the high-frequency spectrum, which causes the prediction to differ from the actual measured result.

As black-box noise prediction is a measurement-based method, the measurement results are very important to noise prediction. The inherent switching fluctuation in a dc–dc converter affects not only the prediction accuracy of the noise source model but also the noise spectrum [21]. The converter's inherent jitter causes the detected peak in the conducted noise to be several decibels larger than the averaged noise. The idea here comes from the frequency modulation technique [24], [25], [26] based on Carson's rule [27]. The peak amplitude occurs under the condition of no fluctuation, whereas the averaged amplitude reflects the condition with fluctuation. The fluctuation spreads the peak spectrum to the sideband without influencing the total noise power. We previously proposed a method, based on this hypothesis, to predict the peak magnitude of the noise and determine the noise reduction by using the frequency modulation technique [28].

In [28], we assumed that the inherent jitter in a dc–dc converter should have the same effect as the frequency modulation technique usually used for the digital circuit to reduce the EMI at higher frequencies. The frequency modulation technique introduces the controlled jitter in the time-domain switching signal to spread the energy to harmonics. The technique was then applied to estimate noise reduction caused by the dc–dc converter's inherent jitter effect and predict the averaged conducted emissions.

Although the predicted spectrum agreed to some extent with the measured one, the technique was not judged suitable to evaluate the inherent jitter effect because the switching fluctuation distribution of a dc–dc converter is different from that introduced with the frequency modulation technique, which results from the difference between the random jitter and deterministic jitter. Since the jitter distribution is different, so is the reduction value caused by the jitter. Thus, we propose an experimental-based method to assess noise reduction through trigger-source measurement.

To obtain the actual noise spectrum, the reduction as well as the "ideal" noise spectrum with no fluctuation is required. Therefore, we proposed a method for decomposing a measured time-domain noise signal without fluctuation into ripple noise and turn-ON and turn-OFF spike noises to avoid accuracy degradation in parameter identification [29]. The waveform decomposition method can avoid the undesired averaging effect in time-domain measurement and predict the actual (peak) noise level. This waveform decomposition method for peak detection can be used to predict noise spectra without switching fluctuation within a 3-dB prediction error up to 200 MHz. However, the work in [29] is a one-page abstract, so the explanation of the detailed process was omitted due to the page limitation. In this article, therefore, the waveform decomposition method is explained in detail to predict the actual noise spectrum.

In summary, the inherent jitter behaves similarly to works the frequency modulation technique and reduces the noise amplitude at higher frequencies. On the basis of the hypothesis that the inherent jitter has the same effect as the frequency modulation technique, we first estimate the reduction through the experimental approach using the spectrum caused by switching fluctuation. To obtain the actual noise spectrum, in reality, we need the reduction as well as the "ideal" noise spectrum with no fluctuation. We then obtain the "ideal" spectrum by using the waveform decomposition method proposed in [29]. Finally, we subtract the noise reduction from the "ideal" noise spectrum and obtain the actual noise spectrum.

The rest of this article is organized as follows. Section II examines the switching fluctuation in a dc–dc converter and its influence on noise measurement. Section III introduces our noise source model and the waveform decomposition method. Section IV describes an experimental validation and noise prediction without switching fluctuation, and Section V then validates the noise reduction due to switching fluctuation. Finally, we give a few concluding remarks in Section VI.

II. Switching Fluctuation Effect on Measured Noise Signal

The prediction accuracy of our model is highly correlated to oscilloscope measurement. For measuring stochastic conducted emissions, the averaging mode is usually used to eliminate jitter. However, part of the noise component is also removed, which makes it necessary to investigate which part and by how much the noise is reduced.

In this section, we first examine the switching fluctuation distribution in a dc–dc converter, and we then show the noise spectra with and without using the averaging mode. Next, we investigate the triggered and untriggered spike signals. Finally, we describe our method to determine the noise reduction due to fluctuation.

A. Switching Fluctuation Distribution

First, we measured the distribution of switching fluctuation. The main causes of the switching fluctuation in a dc–dc converter are considered to include nonlinearity of the sawtooth slope of the analog pulsewidth modulation (PWM) controller, ground noise coupling between the power and control stages, insufficient PWM resolution in the digital controller, and component selection and placement. For this article, a dc–dc buck converter (Rohm, BD9G341EFJ-EVK-101) with a 10-Ω load was used for evaluation. The input voltage was 18 V, and the output voltage was 5 V. Two passive 10:1 probes (KEYSIGHT N2894 A with 10-MΩ input resistance and 9.5-pF input capacitance) were used for measuring the input and output noise while another one was used for measuring the reference signal, as shown in Fig. 3. The signal at the switching node of the dc–dc converter served as the reference signal. The switching frequency was 200 kHz. The trigger was applied to the switching-node voltage, and the trigger level was set to 9 V, which was half the maximum switching-node voltage of 18 V in this study.

Fig. 4(a) shows the trigger source measurement positions in the time-domain switching signal from the switching node, and Fig. 4(b) shows an oscilloscope histogram of the jitter distribution at the indicated measurement position in Fig. 4(a). The results indicate that the switching fluctuation can be considered to have a normal distribution. The full width at half maximum (FWHM) is 22 ns; therefore, the standard deviation σ is calculated as 9.34 ns because FWMH $= 2\sqrt{2}\sigma$.

The reason for the random distribution is that the measured result can be seen as total jitter and can thus be split into random jitter (i.e., a random distribution) and deterministic jitter. Accordingly, by the central limit theorem in probability, the total jitter tends to resemble a Gaussian distribution.

B. Averaging Effect on Noise Signal

Switching fluctuation makes noise measurement time-variant, which means that the time-invariant black-box (EMI) model is inapplicable. Generally, the averaging mode is used for noise measurement to eliminate switching fluctuation but it leads to another problem during such measurement.

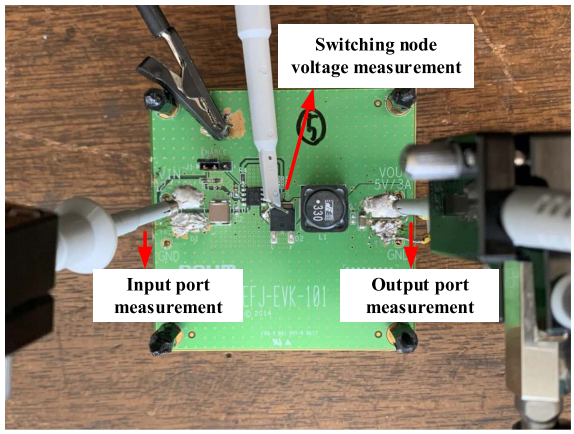

(a)

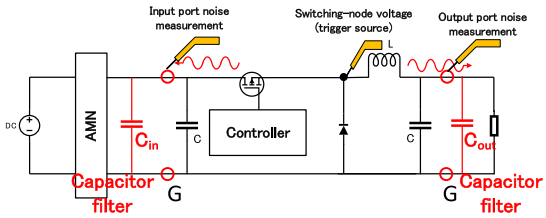

(b)

Fig. 3. Switching fluctuation measurement results. (a) DC–DC buck under measurement. (b) Measurement setup on the converter.

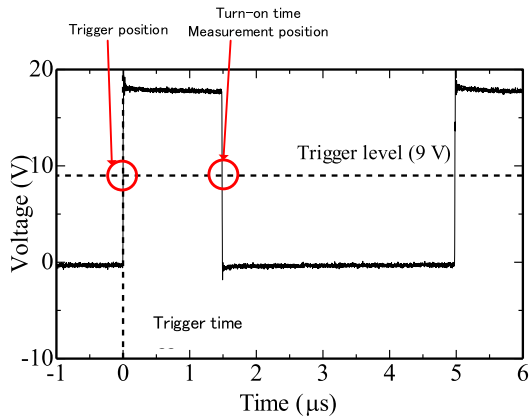

(a)

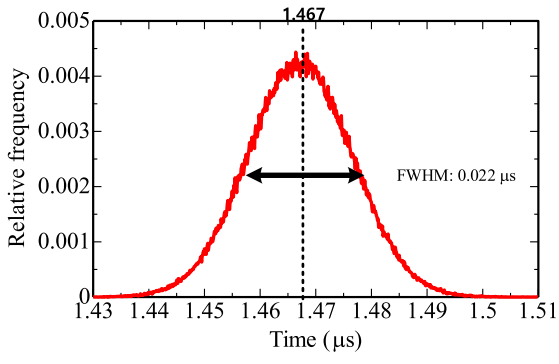

(b)

Fig. 4. Switching fluctuation measurement results. (a) Switching fluctuation measurement waveform. (b) Switching fluctuation distribution.

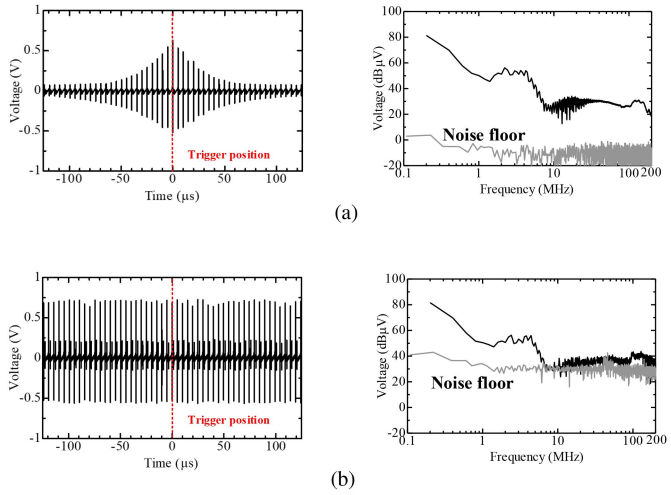

Fig. 5. Input noise signal measured by an oscilloscope. (a) Noise signal averaged 1024 times. (b) Noise signal without averaging.

Hence, we compared the measured noise signals with and without averaging in the input port's time domain and frequency domain. Although a power converter is a nonlinear, time-variant network, we assume the noise-source equivalent circuit model to be a linear time-invariant circuit when we approximate the conducted noise of the dc–dc converter. Averaging can improve the measurement accuracy but the oscilloscope averaging mode eliminates random noise and makes the measured signal approximately time-invariant. Moreover, the averaging acquisition mode removes a significant amount of conducted noise at higher frequencies.

Here, we took the input time-domain signal as an example. We set the oscilloscope (Keysight DSOS104 A) to ac voltage measurement with a rising trigger slope. Fig. 5(a) shows the time-domain signal and the frequency-domain spectrum averaged over 1024 times when the trigger was set to the time-zero position. Fig. 5(b) shows the measured result without averaging and the frequency-domain spectrum after the application of a fast Fourier transform (FFT). The random noise in the frequency-domain spectrum was approximately 40 dB but parts of the averaged noise signal were removed by averaging. In particular, a reduction of about 10 dB can be observed in the range of 10–200 MHz. As a result, even though averaging improves the measurement accuracy at lower frequencies, the noise signal degrades at higher frequencies because of the actual noise of the dc–dc converter.

Thus, there is a tradeoff between measuring the actual noise and averaging the measurements. An interference signal with a high signal-to-noise ratio (SNR) can be measured with the averaging mode but the high-frequency noise amplitude will be lower than the actual noise. In contrast, a stochastic interference signal measured without averaging has a low SNR and cannot be used with the linear approach. As a result, we need an approach to maintain the SNR without degrading EMI measurement.

C. Triggered and Untriggered Spike Noise Signals

We next studied the triggered and untriggered spike noise signals; here, the signal from the switching node served as a reference signal, and the trigger edge was rising. Fig. 6 shows 10 samples of zoomed (a) turn-ON and (b) turn-OFF spike noise signals without averaging. The results indicate that the triggered turn-ON spike noise signal has no switching fluctuation, whereas the turn-OFF spike noise signal does.

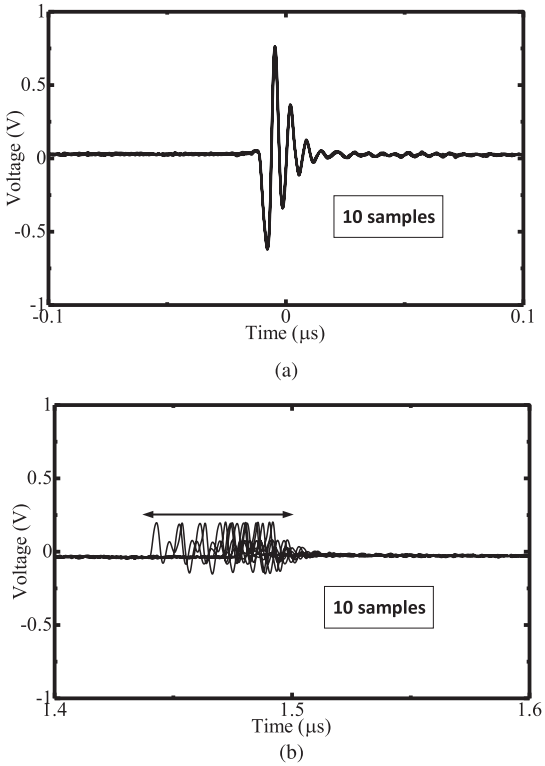

Fig. 6. Spike noise with and without triggering. (a) Triggered turn-ON noise. (b) Untriggered turn-OFF noise.

As a result, only the triggered turn-ON spike signal and ripple noise (i.e., noise below 10 MHz) meet the accuracy requirement. That is, because the averaging mode only keeps the periodic noise signal, much of the turn-OFF noise in Fig. 6(b) is removed, which makes the prediction inaccurate. Hence, as averaging improves the measurement accuracy only for the triggered signal and degrades the accuracy of the untriggered signal, the prediction accuracy will be improved by decomposing the noise signal and acquiring only the triggered noise signal to identify the noise parameter.

The basic idea for waveform decomposition is to extract the ripple noise and spike noise to avoid the switching fluctuation influence. The general process to extract the decomposed noise signal will be introduced in Section III.

D. Switching Fluctuation Effect on Noise Spectrum

We assume that the inherent fluctuation of the dc–dc converter spreads the noise power spectrum, which is similar to the principle of the frequency modulation technique. Even though that technique is usually used for EMI reduction, consideration of Carson's rule can help us understand how switching fluctuation affects the noise spectrum. The frequency modulation technique introduces controlled jitter into a time-domain signal to deal with the converter not having perfect periodic behavior and thus

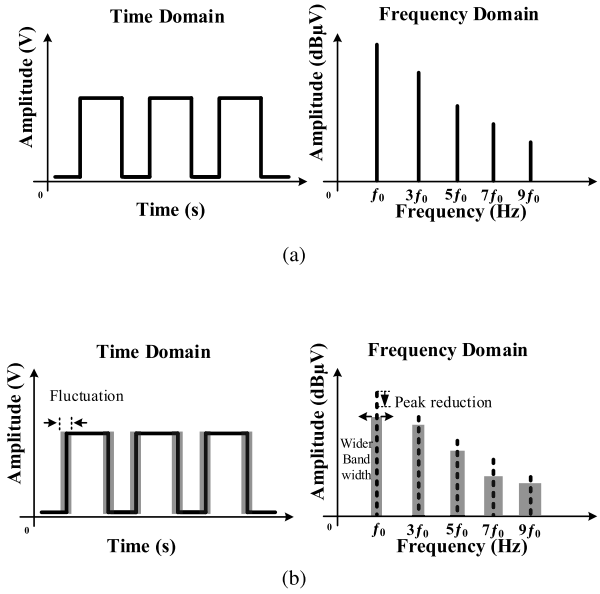

Fig. 7. Time and frequency domains for an ideal signal and a signal with switching fluctuation. (a) Ideal switching signal. (b) Frequency-modulated switching signal.

spreading the harmonic power over a bandwidth. The bandwidth depends on the introduced jitter characteristics.

Fig. 7 shows the time domain and frequency domain of an ideal switching signal and a frequency-modulated switching signal. For the unmodulated switching signal in Fig. 7(a), which has no switching fluctuation at the switching frequency f_0, each harmonic is narrow and close to the peak amplitude. For the modulated switching signal with switching fluctuation in Fig. 7(b), the energy of each harmonic is spread over a wider bandwidth. Therefore, the peak amplitude at each harmonic is reduced.

As the spike noise signal is caused by a high-dv/dt switching clock, we can assume that the peak spike noise is due to the ideal switching condition without fluctuation. The ideal turn-ON time is about 1.467 μs, which is the mean of the normal distribution shown in Fig. 4. Moreover, the actual spectrum is spread by the inherent switching fluctuation. The actual turn-ON time thus has variation, which follows a normal distribution.

From the above consideration, we can study noise reduction by comparing ideal switching waveforms (without fluctuation) and actual switching signals (with fluctuation). To obtain a switching waveform with fluctuation, we measured the actual switching signal with an oscilloscope, as shown in Fig. 8(a). The sampling rate was 1 GS/s, and 100 periods of the switching signal were measured first. The measurement position was the switching node shown in Fig. 3. The turn-ON time varied, and the time deviation distribution followed that shown in Fig. 4(b). To obtain a switching waveform without fluctuation, a one-period switching signal was extracted from the measured waveform, whose turn-ON time was close to 1.467 μs, and the waveform was then duplicated 100 times. As a result, we obtained a waveform like that shown in Fig. 8(b). Fig. 8(c) shows the FFT result obtained in MATLAB. The switching signal with the time deviation spectrum has a lower amplitude than without time

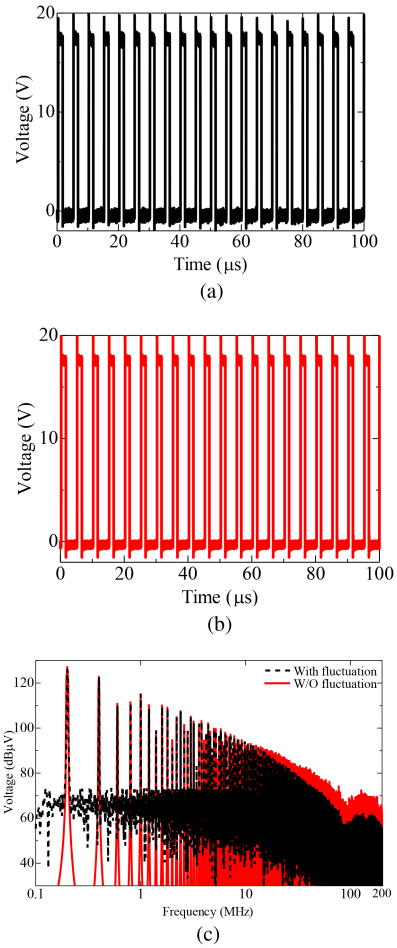

Fig. 8. Switching signal waveforms and spectra. (a) Switching signal with fluctuation. (b) Switching signal duplicated from one period without fluctuation. (c) Spectrum comparison (100 periods).

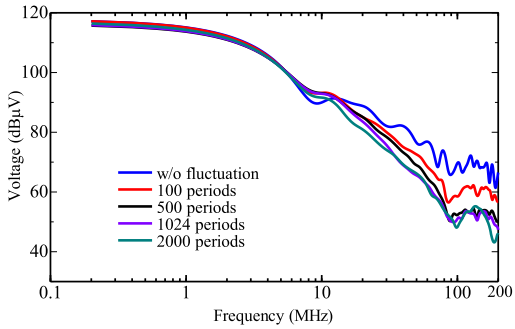

Fig. 9. Envelope spectra for different numbers of switching periods.

deviation from 10 to 200 MHz. The difference has a positive correlation with the frequency.

The duration of the switching signal is the main factor that influences the spectrum amplitude in the spike noise frequency range. A short duration cannot contain the total reduction due to fluctuation, whereas the spectrum finally converges to the amplitude with a long enough waveform. Fig. 9 shows the envelope spectra for different durations, which indicate that the envelope converges at about 1000 periods of the switching waveforms. The noise reduction can be calculated from the differences

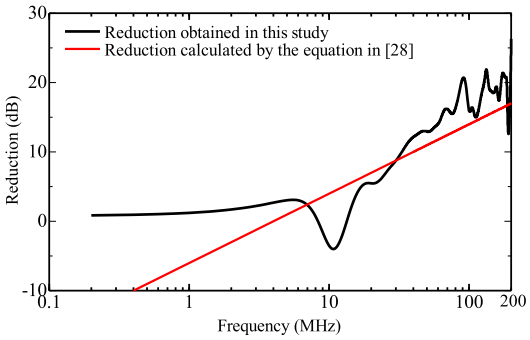

Fig. 10. Noise signal reduction due to switching fluctuation.

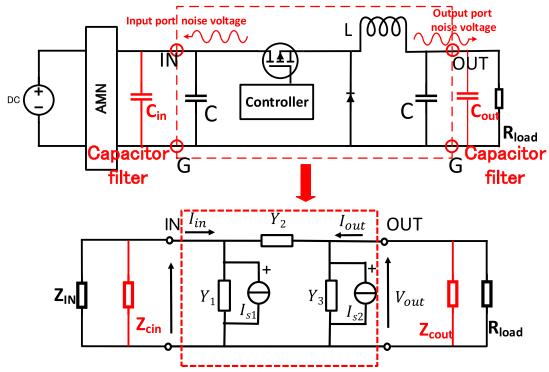

Fig. 11. Two-port equivalent circuit model for a dc–dc converter.

between the switching signal spectra with fluctuation, by using 1024 switching periods, which is the same as the averaging by the oscilloscope and without fluctuation. The calculated result is shown in Fig. 10, and it reveals that the noise spectrum is reduced above 10 MHz, which is the spike noise range. In other words, the switching fluctuation has no influence on the ripple noise, as was shown in Fig. 5. In Fig. 10, the red curve indicates the noise-reduction spectrum used in our previous study [28]. The red spectrum is a good approximation but does not match the reduction obtained in this study. Since the switching fluctuation distribution of a dc–dc converter is different from that introduced with the frequency modulation technique, we applied the experimental-based method to decrease the prediction errors.

In this section, we have studied the noise reduction due to switching fluctuation. The results showed that ripple noise is not affected by fluctuation while the spike noise spectrum is reduced by at least several decibels from the peak amplitude. Hence, in the next section, we introduce a waveform decomposition method that can predict the peak amplitude spectrum. The averaged noise spectrum can then be predicted by combining the two methods described in this section and the next one.

III. Noise Source Equivalent Circuit Model and Parameter Identification Procedure

In this section, we first define the model structure, the model parameterization process, and then introduce the waveform decomposition method.

A. Model Definition

Fig. 11 shows a model based on a Norton equivalent circuit that includes three noise admittances and two noise current sources. This kind of two-port model separates the load from the model, making it possible to study noise-source equivalent circuit parameters with different load values. Instead of being extended to a load-dependence model, the model is limited to DM noise prediction, because it does not involve the ground wire, i.e., the system ground. In general, CM noise is generated by the system ground and the surrounding metals, which our model does not address. In practice, onboard measurement can keep the mode conversion between the common and DMs small. The model only focuses on the DM noise of input-port noise $\dot{V}_{\rm in}$ and output-port noise $\dot{V}_{\rm out}$.

In [15], the circuit equations with the five model parameters $(\dot{Y}_1, \dot{Y}_2, \dot{Y}_3, \dot{I}_{\rm s1}, \dot{I}_{\rm s2})$, were derived from the noise model shown in Fig. 11 on the basis of Kirchhoff's current law and expressed as follows:

$$\begin{bmatrix} \dot{I}_{\rm in} \\ \dot{I}_{\rm out} \end{bmatrix} = \begin{bmatrix} \dot{V}_{\rm in} & \dot{V}_{\rm in} - \dot{V}_{\rm out} & 0 & -1 & 0 \\ 0 & -\dot{V}_{\rm in} - \dot{V}_{\rm out} & \dot{V}_{\rm out} & 0 & -1 \end{bmatrix} \begin{bmatrix} \dot{Y}_1 \\ \dot{Y}_2 \\ \dot{Y}_3 \\ \dot{I}_{\rm s1} \\ \dot{I}_{\rm s2} \end{bmatrix}. \quad (1)$$

To identify the model parameter, the input port current $\dot{I}_{\rm in}$ and output port current $\dot{I}_{\rm out}$ as well as $\dot{V}_{\rm in}$ and $\dot{V}_{\rm out}$ are required under different conditions: normal condition with no filter and attenuated condition with a capacitor, as shown in red in Fig. 11. The capacitor filter is used because it will affect neither the input dc voltage nor the duty cycle of the dc–dc converter.

For the normal condition, $\dot{I}_{\rm in}$ and $\dot{I}_{\rm out}$ are calculated using the following equations:

$$\dot{I}_{\rm in} = -\dot{V}_{\rm in}/Z_{\rm IN} \quad (2)$$

$$\dot{I}_{\rm out} = -\dot{V}_{\rm out}/R_{\rm load} \quad (3)$$

where $Z_{\rm IN}$ denotes the impedance of our handmade artificial mains network circuit. The circuit diagram and impedance magnitude are shown in Fig. 12.

For the attenuated condition, capacitor filters with equal capacitance are inserted into the input and output ports of the dc–dc converter. We then measure the filtered input-port noise $\dot{V}'_{\rm in}$ and output-port noise $\dot{V}'_{\rm out}$, and calculate input-port and output-port current by

$$\dot{I}'_{\rm in} = -\dot{V}'_{\rm in}/(Z_{\rm IN} \parallel Z_{\rm cin}) \quad (4)$$

$$\dot{I}'_{\rm out} = -\dot{V}'_{\rm out}/(R_{\rm load} \parallel Z_{\rm cout}) \quad (5)$$

where $Z_{\rm cin}$ and $Z_{\rm cout}$ are, respectively, the impedances of the filter inserted in the input and output-ports including ESL and ESR. The measurement process and filter information are presented in the next section.

To solve (1), it is necessary to obtain noise signals under at least three different conditions. Accordingly, the conducted noise can be filtered by changing the capacitances at the input and output ports to obtain attenuated noise signals. In each measurement, we obtain one pair of equations. After three-time

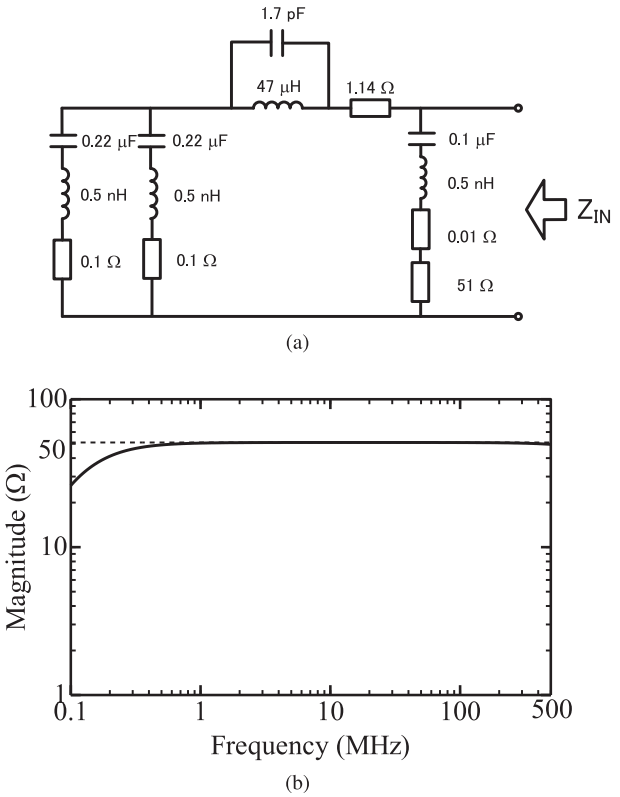

Fig. 12. Artificial mains network. (a) Artificial mains network circuit diagram. (b) Artificial mains network circuit impedance.

measurements, an overdetermined system of equations is obtained. The ordinary least squares method is applied to find a set of solutions to the overdetermined system.

B. Model Parameterization Process

As the model contains five unknown parameters, three different measurements are necessary to solve $(\dot{Y}_1, \dot{Y}_2, \dot{Y}_3, \dot{I}_{s1}, \dot{I}_{s2})$. The insertion loss method [7] was used to obtain different measurements by filtering the conducted noise with capacitors (GRM31CR71A475KA01) soldered in parallel. It is applied to solve the noise source impedance due to the EMI filter insertion loss. In [7], only the source impedance was solved; here, however, we adapted Norton's equivalence theorem and extended the method to a two-port noise-source equivalent circuit. To solve (1), we measured one unfiltered noise case and two filtered noise cases for six equations.

The input port noises $\dot{V}_{in}$ and $\dot{V}_{out}$ were measured in the time domain by an oscilloscope and then transformed by an FFT into the frequency spectrum. Oscilloscopes are widely used for black-box EMI modeling, as time-domain measurements can provide phase information to identify the model parameters for an equivalent circuit model, including multiple noise sources. According to the work in [30], the difference between FFT results and frequency measurements can be ignored when the dc–dc converter switching frequency is much higher than the resolution bandwidth in the EMI standard. The measurement in the current work satisfies this condition.

TABLE I
MEASUREMENT CONDITIONS

	Condition 1	Condition 2
Sampling rate	1 Gs/s	10 Gs/s
Measurement time	250 µs	1 µs
Averaging times	1024	1024

In addition, six equations were obtained from one pair of no-filter measurements and two pairs of filtered measurements with two and four capacitors, respectively, having the same value and soldered in parallel. The least-squares method was used to calculate the overdetermined system. [15].

C. Waveform Decomposition Method

In this method, we divide the time-domain signal into three parts and build a noise model for each one, as shown in Fig. 13. The time-domain noise signal of the dc–dc converter is decomposed into ripple noise (below 10 MHz), turn-ON spike noise, and turn-OFF spike noise (10–200 MHz). This method predicts the peak noise amplitude without fluctuation.

To predict noise spectra accounting for switching fluctuation, we consider the fluctuation spread of the power at the harmonic to the sideband; thus, the peak spectrum is reduced by at least several decibels. As explained in Section II, the reduction can be calculated from the difference between the actual switching signal spectrum and the ideal switching signal spectrum of the dc–dc converter. The specific process is explained in Section IV.

Fig. 14 illustrates the process of the waveform decomposition method, and Table I lists the measurement conditions. For the three decomposed noise components of the time-domain signal—that is, the ripple noise $n_1(t)$, the turn-ON spike noise $n_2(t)$, and the turn-OFF spike noise $n_3(t)$—the following equation holds:

$$n(t) = n_1(t) + n_2(t) + n_3(t)\ . \tag{6}$$

The time-domain signal expressed by (6) can then be transformed into a frequency spectrum:

$$N(f) = N_1(f) + N_2(f) + N_3(f) \tag{7}$$

$$N_i(f) = \mathrm{FFT}[n_i(t)] \quad (i = 1, 2, 3). \tag{8}$$

As we decompose the noise signal into three parts, the noise models for prediction are also divided into three models. Therefore, we need six noise prediction models to account for each port [28], [29].

IV. EXPERIMENTAL SETUP AND MODEL EVALUATION

In the measurement setup shown in Fig. 15, a handmade artificial main network of which the circuit diagram and impedance with frequency are shown in Fig. 12 was used to block the noise from the dc power supply (KENWOOD PW18-1.8AQ ±18 V/1.8 A). An oscilloscope (Keysight DSOS104 A with 1 GHz bandwidth, 20 GSa/s) with three high-impedance passive 10:1 probes (KEYSIGHT N2894 A 700 MHz with 10-MΩ input resistance and 9.5-pF input capacitance) were used for measurement: One to measure the triggered signal from

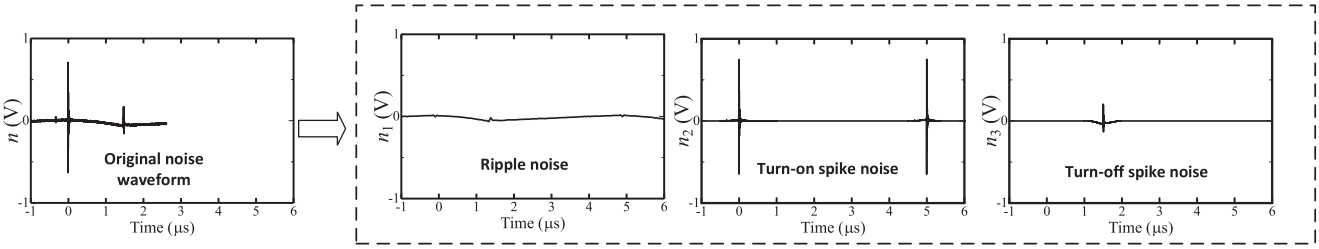

Fig. 13. Waveform decomposition for dividing time-domain signal to three parts and building the noise model.

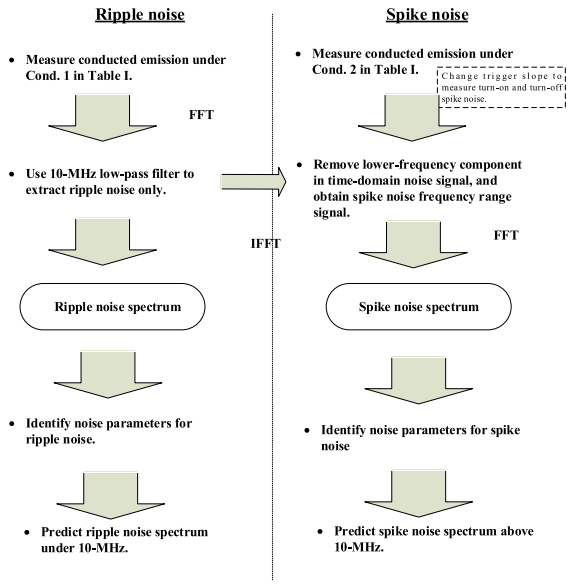

Fig. 14. Process of the waveform decomposition method.

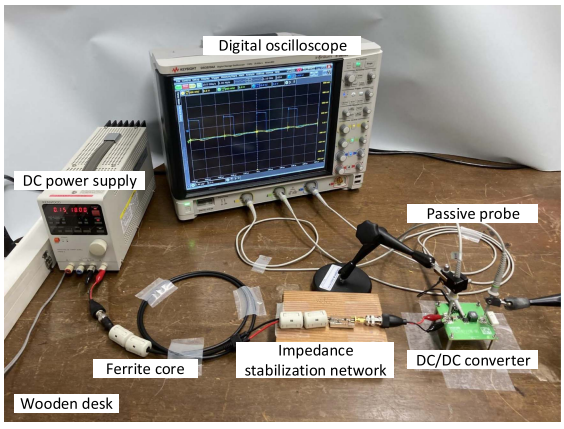

(a)

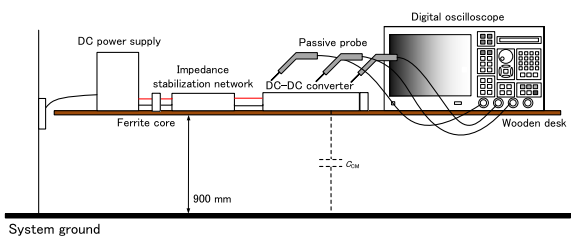

(b)

Fig. 15. Measurement setup. (a) Test bench setup. (b) Overview of test bench setup.

the switching node of the dc–dc converter, and two to measure the input and output port noise. The operating conditions of the dc–dc buck converter were the same as the setting for measuring the distribution of the switching fluctuation as described in Section II-A.

To obtain the waveform via the waveform decomposition method, the ripple noise was obtained by using a 10-MHz low-pass filter of built-in matlab function $designfilt$. The sampling rate was 1 GS/s, and the measurement time was 250 μs, averaged 1024 times. The turn-ON and turn-OFF spike noise were measured by setting the trigger to the rising and falling slopes, respectively, of the reference signal. The sampling rate was 10 GS/s to obtain enough points in a short time, and the measurement time was 1 μs, averaged 1024 times. Moreover, the noise floor was measured at a setting of 200 mV/div, which was the same as the measurement setting for the ripple noise and spike noise.

The noise parameters were identified for each decomposed noise spectrum. A 4.7-μF filter capacitor (GRM31CR71A475KA01) with a 5-m Ω ESR and a 0.5-nH ESL was soldered in parallel at each converter port for parameter identification. The filter cases for parameter identification were "not applicable" (N/A), 9.4 μ F (two capacitors in parallel), and 19.8 μF (four capacitors in parallel). The conduction emission measured in the 4.7-μF filter case was used for evaluation. Noise prediction was performed for each decomposed noise spectrum (i.e., the low-frequency ripple noise and the high-frequency spike noise).

Fig. 16 shows the parameter identification results. Specifically, the magnitudes of the ripple noise, turn-OFF spike noise, and turn-ON spike noise are shown in red, blue, and green, respectively. The ripple noise and spike noise were recomposed via (7). Fig. 17 shows noise spectra comparisons between the prediction and measurement results, for the input port and output port, respectively. In each of these figures, panels (a) and (b) show the ripple noise, turn-ON spike noise, and turn-OFF spike noise spectra. As seen in the figures, the prediction difference was within 3 dB in the range of up to 200 MHz. The turn-OFF spike noise was overwhelmed by the turn-ON spike noise from 10 to 200 MHz.

V. Spectrum Prediction With Switching Fluctuation

The prediction results in Section IV indicated the spectra of a decomposed signal without switching fluctuation. The prediction results were close to the peak detected spectrum but our goal is to predict the averaged spectrum obtained by measurement.

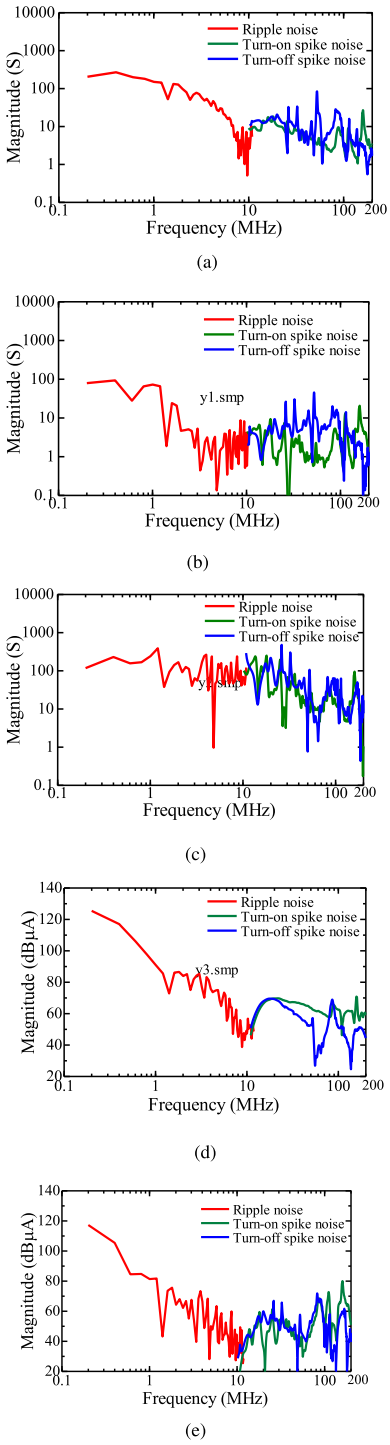

Fig. 16. Identified noise parameters. (a) *Y1*. (b) *Y2*. (c) *Y3*. (d) *Is1*. (e) *Is2*.

As the ripple noise is not affected by the switching action, the reduction process only applies to the switching noise (i.e., spike noise). Moreover, the prediction result showed that the turn-OFF spike noise is smaller than the turn-ON spike noise. In other words, because the turn-ON spike noise spectrum overwhelms the turn-OFF spike noise during measurement, we only describe the results for the turn-ON spike noise here.

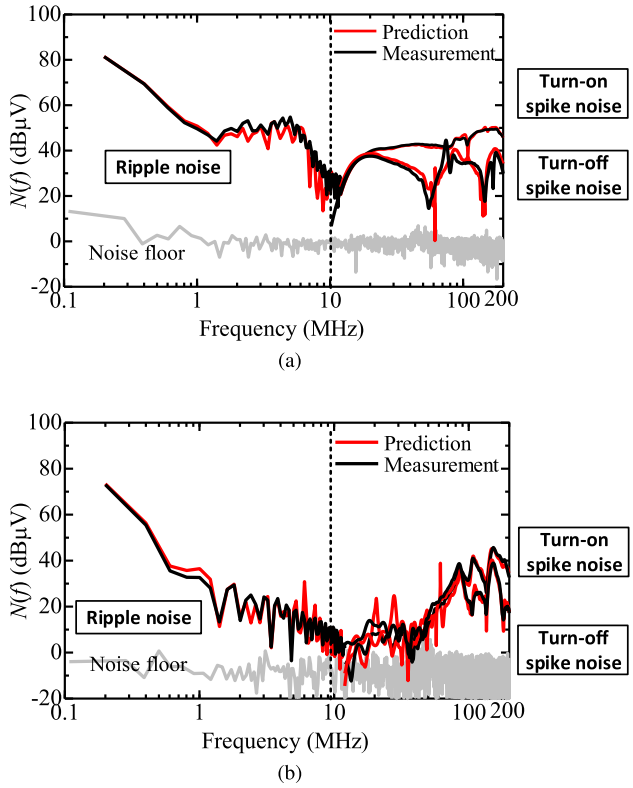

Fig. 17. Comparison between the prediction and measurement result. (a) Input-port noise. (b) Output-port noise.

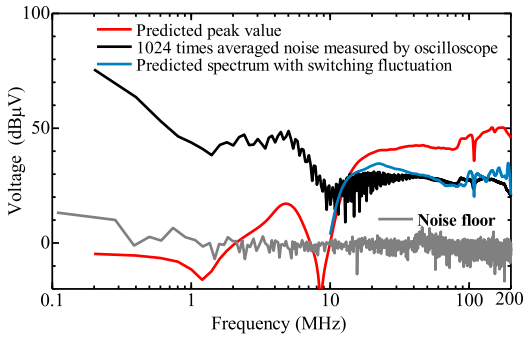

Fig. 18. Noise prediction accounting for switching fluctuation.

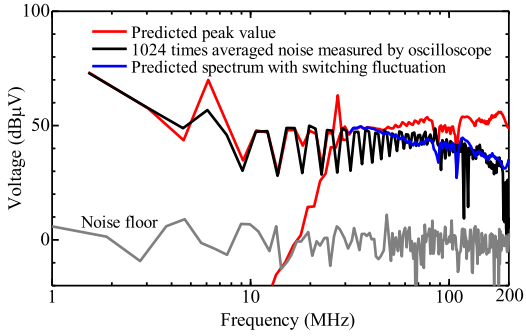

Fig. 19. Noise prediction accounting for switching fluctuation in boost converter.

Based on the hypothesis that noise reduction at higher frequencies is caused by switching fluctuation, the averaged noise spectrum can be obtained by using a semiempirical method to subtract the reduction from the peak detected noise predicted using the waveform decomposition method without switching fluctuation.

The turn-ON spike noise spectrum above 10 MHz was thus predicted by subtracting the reduction shown in Fig. 10. Fig. 18 shows the predicted spectrum in blue in comparison with the measured spectrum averaged 1024 times in red, with the peak spectrum in black. The results show good agreement between the measurement and predicted spectra.

The proposed approach is not independent of the type of a dc–dc converter. To validate this, the approach was also applied for predicting the conducted emissions from a boost-type converter. Fig. 19 shows the noise prediction result and the good agreement between the measured and predicted spectra, where the turn-OFF spike noise was used for prediction because the turn-ON spike noise is overwhelmed by such noise. The details are outlined in the Appendix.

VI. Conclusion

In this article, we predicted both the averaged noise and the detected peak in the conducted emission from a dc–dc converter. We have so far proposed our hypothesis that the inherent jitter caused by switching fluctuation of the dc–dc converter reduces the noise amplitude at higher frequencies and verified it using the semiempirical method. We then combined the black-box model with the waveform decomposition method to eliminate switching fluctuation during time-domain measurement.

We investigated the influence of switching fluctuation on noise during the converter's operation. The fluctuation was assumed to be a frequency modulation that spread the noise spectrum of an ideal switching clock. The spike noise power was spread by fluctuation, and the reduction was calculated via the ideal switching waveform and the actual switching waveform.

We then proposed a waveform decomposition method that decomposes the whole time-domain noise signal waveform into ripple noise, turn-ON spike noise, and turn-OFF spike noise. Through this method, we could avoid the switching fluctuation effect during parameter identification for the noise source equivalent model. The method's prediction result was close to the peak amplitude, and the error was within 3 dB up to 200 MHz. The averaged noise was calculated from the peak value and the noise reduction due to switching fluctuation, and the predicted averaged spectrum noise had good agreement with the measured noise spectrum.

Appendix

A dc–dc boost converter (Analog Devices, DC2186A-A) with a 1.5-MHz switching frequency was used for evaluation when the input and output voltages were, respectively, 9 and 12 V and the load was 30 Ω. The noise properties of the boost converter are different from the buck converter. The turn-OFF noise is larger than the turn-ON noise in the boost converter. Thus, we predicted the boost-converter turn-OFF noise accounting for switching fluctuation.

The experiment and prediction processes are the same as that for the buck converter, except for the filter capacitor values and the low-pass filter stopband of the built-in MATLAB function. Since the boost converter's switching frequency is 1.5 MHz higher than that of the buck converter we used, the ripple noise frequency range was found to be 20 times the switching frequency, and the low-pass filter stopband was 30 MHz. A 1-μF filter capacitor (GRM42-6F105Z25) with a 0.14-mΩ ESR and 1.55-nH ESL was used for noise parameter identification.

References

[1] H. Heeb and A. E. Ruehli, "Three-dimensional interconnect analysis using partial element equivalent circuits," *IEEE Trans. Circuits Syst. I: Fundam. Theory Appl.*, vol. 39, no. 11, pp. 974–982, Nov. 1992.

[2] J. Meng, W. Ma, Q. Pan, Z. Zhao, and L. Zhang, "Noise source lumped circuit modeling and identification for power converters," *IEEE Trans. Ind. Electron.*, vol. 53, no. 6, pp. 1853–1861, Dec. 2006.

[3] Q. Liu, F. Wang, and D. Boroyevich, "Modular-terminal-behavioral (MTB) model for characterizing switching module conducted EMI generation in converter systems," *IEEE Trans. Power Electron.*, vol. 21, no. 6, pp. 1804–1814, Nov. 2006.

[4] A. C. Baisden, D. Boroyevich, and F. Wang, "Generalized terminal modeling of electromagnetic interference," *IEEE Trans. Ind. Appl.*, vol. 46, no. 5, pp. 2068–2079, Sep./Oct. 2010.

[5] H. Bishnoi, A. C. Baisden, P. Mattavelli, and D. Boroyevich, "Analysis of EMI terminal modeling of switched power converters," *IEEE Trans. Power Electron.*, vol. 27, no. 9, pp. 3924–3933, Sep. 2012.

[6] H. Bishnoi, P. Mattavelli, R. Burgos, and D. Boroyevich, "EMI behavioral models of DC-fed three-phase motor drive systems," *IEEE Trans. Power Electron.*, vol. 29, no. 9, pp. 4633–4645, Sep. 2014.

[7] D. Zhang, D. Y. Chen, M. J. Nave, and D. Sable, "Measurement of noise source impedance of off-line converters," *IEEE Trans. Power Electron.*, vol. 15, no. 5, pp. 820–825, Sep. 2000.

[8] M. Foissac, J.-L. Schanen, and C. Vollaire, ""Black box" EMC model for power electronics converter," in *Proc. IEEE Energy Convers. Congr. Expo.*, 2009, pp. 3609–3615.

[9] G. Frantz, D. Frey, J. L. Schanen, B. Revol, H. Bishnoi, and P. Mattavelli, "EMC models for power electronics: From converter design to system level," in *Proc. IEEE Energy Convers. Congr. Expo.*, 2013, pp. 4247–4252.

[10] T. J. Donnelly, S. D. Pekarek, D. R. Fudge, and N. Zarate, "Thévenin equivalent circuits for modeling common-mode behavior in power electronic systems," *IEEE Open Access J. Power Energy*, vol. 7, no. 1, pp. 163–172, 2020.

[11] B. Czerniewski, J.-L. Schanen, H. Chazal, P. Zanchetta, and C. F. de Freitas, "Identification and validation of a non symmetrical system level EMC model for power electronics converter," in *Proc. IEEE Energy Convers. Congr. Expo.*, 2021, pp. 2859–2865.

[12] B. Kerrouche, M. Bensetti, and A. Zaoui, "New EMI model with the same input impedances as converter," *IEEE Trans. Electromagn. Compat.*, vol. 61, no. 4, pp. 1072–1081, Aug. 2019.

[13] H. Zhang and S. Wang, "EMI noise source modeling based on network theory for power converters with mixed-mode characterization," in *Proc. IEEE Appl. Power Electron. Conf. Expo.*, 2018, pp. 984–991.

[14] Y. Osaki, Y. Yano, K. Iokibe, and Y. Toyota, "Parameter identification of noise-source linear equivalent circuit of DC–DC converter and its evaluation," in *Proc. APEMC*, 2017, Art. no. 217.

[15] T. Uematsu, Y. Osaki, Y. Yano, K. Iokibe, and Y. Toyota, "Improvement of prediction accuracy of noise-source equivalent-circuit model based on parameter extraction by port voltage/current measurement," in *Proc. Joint Int. Symp. Electromagn. Compat. Asia-Pacific Int. Symp. Electromagn. Compat.*, 2019, Art. no. 199.

[16] S. Zhang, T. Uematsu, K. Iokibe, and Y. Toyota, "Two-port noise source equivalent circuit model for DC/DC buck converter with consideration of load effect," in *Proc. Int. Symp. Electromagn. Compat.-EMC EUROPE*, 2020, pp. 1–4.

[17] H. M. Rebholz, S. Tenbohlen, and W. Köhler, "Time-domain characterization of RF sources for the design of noise suppression filters," *IEEE Trans. Electromagn. Compat.*, vol. 51, no. 4, pp. 945–952, Nov. 2009.

[18] A.-M. Sánchez, S. A. Pignari, J.-R. Regué, and M. Ribó, "Device modeling for nonstationary conducted emissions based on frequency- and time-domain measurements," *IEEE Trans. Electromagn. Compat.*, vol. 54, no. 4, pp. 738–746, Aug. 2012.
[19] R. Trinchero, I. S. Stievano, and F. G. Canavero, "EMI prediction of switching converters," *IEEE Trans. Electromagn. Compat.*, vol. 57, no. 5, pp. 1270–1273, Oct. 2015.
[20] R. Trinchero, I. S. Stievano, and F. G. Canavero, "Enhanced time-invariant linear model for the EMI prediction of switching circuits," *IEEE Trans. Electromagn. Compat.*, vol. 62, no. 5, pp. 2294–2302, Oct. 2020.
[21] G. Shen et al., "Terminal modeling of DC–DC converters with stochastic behavior," *IEEE Trans. Electromagn. Compat.*, vol. 60, no. 6, pp. 2011–2018, Dec. 2018.
[22] L. Wan et al., "Assessment of validity conditions for black-box EMI modelling of DC/DC converters," in *Proc. IEEE Int. Joint EMC/SI/PI EMC Europe Symp.*, 2021, pp. 581–585.
[23] D. Bellan, F. Marliani, S. A. Pignari, and G. Spadacini, "Spectral analysis of conducted emissions of DC/DC converters," in *Proc. IEEE Int. Symp. Electromagn. Compat.*, 2010, pp. 490–494.
[24] F. Lin and D. Y. Chen, "Reduction of power supply EMI emission by switching frequency modulation," *IEEE Trans. Power Electron.*, vol. 9, no. 1, pp. 132–137, Jan. 1994.
[25] J. Balcells, A. Santolaria, A. Orlandi, D. Gonzalez, and J. Gago, "EMI reduction in switched power converters using frequency modulation techniques," *IEEE Trans. Electromagn. Compat.*, vol. 47, no. 3, pp. 569–576, Aug. 2005.
[26] F. Pareschi, R. Rovatti, and G. Setti, "EMI reduction via spread spectrum in DC/DC converters: State of the art, optimization, and tradeoffs," *IEEE Access*, vol. 3, pp. 2857–2874, 2015.
[27] J. R. Carson, "Notes on the theory of modulation," *Proc. Inst. Radio Eng.*, vol. 10, no. 1, pp. 57–64, 1922.
[28] S. Zhang, K. Iokibe, and Y. Toyota, "An approach to predicting conducted noise from DC–DC converter accounting for switching fluctuation," in *Proc. Asia-Pacific Int. Symp. Electromagn. Compat.*, 2021, pp. 1–4.
[29] S. Zhang, T. Uematsu, K. Iokibe, and Y. Toyota, "Noise-source parameter identification considering switching fluctuation of DC–DC converter," in *Proc. IEEE Int. Joint EMC/SI/PI EMC Europe Symp.*, 2021, Art. no. 186.
[30] L. Yang, S. Wang, H. Zhao, and Y. Zhi, "Prediction and analysis of EMI spectrum based on the operating principle of EMC spectrum analyzers," *IEEE Trans. Power Electron.*, vol. 35, no. 1, pp. 263–275, Jan. 2020.

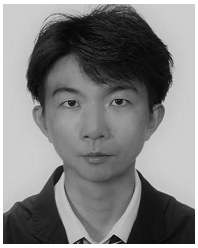

Shuqi Zhang (Student Member, IEEE) received the B.S. degree in electrical engineering from Northeast Electric Power University, Jilin, China, in 2011, and the M.S. degree in power electronics and power drives from Dalian Jiaotong University, Dalian, China, in 2015. He is currently working toward the Ph.D. degree in electronic and information systems engineering with Okayama University, Okayama, Japan.

His research interest includes EMC issue of power converters.

Kengo Iokibe (Member, IEEE) received the B.S., M.S., and Ph.D. degrees in electrical and electronic engineering from Okayama University, Okayama, Japan, in 1997, 1999, and 2005, respectively.

From 2000 to 2002, he was a Research Associate with the Department of Communication Network Engineering, Okayama University. He is currently an Assistant Professor with the Department of Information and Communication Systems, Graduate School of Natural Science and Technology, Okayama University. His recent research interests include information security against side-channel attacks on cryptographic circuits; design of PCB artwork to achieve power integrity, signal integrity, and EMC; imbalance difference modeling for EMC design of electronic systems; and EMC modeling of power converters.

Dr. Iokibe is a member of the Institute of Electronics, Information and Communication Engineers, the Institute of Electrical Engineers of Japan, and the Japan Institute of Electronics Packaging.

Yoshitaka Toyota (Member, IEEE) received the B.S. and M.S. degrees in electrical and electronic engineering from Okayama University, Okayama, Japan, in 1991 and 1993, respectively, and the Ph.D. degree in electronic engineering from Kyoto University, Kyoto, Japan, in 1996.

From 1996 to 1998, he was with Yokogawa Electric Co., Ltd., and in 2005, he was with the Georgia Institute of Technology as an Overseas Research Scholar of the Ministry of Education, Culture, Sports, Science and Technology (MEXT) of Japan. He is currently a Professor with the Graduate School of Natural Science and Technology, Okayama University. His recent research interest includes EMC design for electrical and electronic equipment and systems.

Prof. Toyota is a member of the Institute of Electronics, Information and Communication Engineers, the Japan Institute of Electronics Packaging, the Japan Society of Applied Physics, and the Institute of Electrical Engineers of Japan.